Journal of Alloys and Compounds 506 (2010) 693–697

Contents lists available at ScienceDirect

Journal of Alloys and Compounds

journal homepage: www.elsevier.com/locate/jallcom

Microchemical and microstructural changes of nano-TiN powder during vacuum heat treatment

Ji Xiong[a], Zhixing Guo[a,*], Mei Yang[b], Sujian Xiong[a], Jianzhong Chen[a], Hongyuan Fan[a], Keqin Feng[a], Lan Sun[a], Jun Wang[a], Hui Wang[c]

[a] School of Manufacturing Science and Engineering, Sichuan University, Chengdu 610065, PR China
[b] College of Materials and Chemistry & Chemical Engineering, Chengdu University of Technology, Chengdu 610059, PR China
[c] Analytical & Testing Center, Sichuan University, Chengdu 610065, PR China

ARTICLE INFO

Article history:
Received 28 March 2010
Received in revised form 30 June 2010
Accepted 8 July 2010
Available online 15 July 2010

Keywords:
Vacuum heat treatment
Transmission electron microscopy (TEM)
X-ray photoelectron spectroscopy (XPS)
Nano-TiN powder

ABSTRACT

In the paper, effect of vacuum heat treatment on the chemical composition, microstructure and morphology of nano-TiN powder was investigated. Nano-TiN powders were heat treated in vacuum at 1200 °C for 1 h. XPS, XRD and TEM were used to characterize the surface chemical composition, lattice parameter and morphology of as-received and as-treated nano-TiN. The results showed that the oxygen content adsorbed by nano-TiN powder was largely decreased from 6.64 wt% to 1.18 wt% after heat treatment. The nano-TiN maintained the face-centered cubic structure except a slight decrease of lattice parameter. The average particle size increased from 20 nm to 40 nm, indicating growth of nano-TiN particles during the vacuum heat treatment.

1. Introduction

At present, the Ti(C,N)-based cermets have attracted much attention due to the high hardness, thermal stability, relatively high thermal and electrical conductivities, excellent creep resistance and wear resistance. They have been successfully used for semi-finishing and finishing cutting tools for steel and cast iron [1]. Despite all these advantages, Ti(C,N)-based cermets show poor toughness and thermal shock resistance, which result in brittle fracture at high stresses. In 1970s, TiN was introduced into TiC–Ni–Mo cermets [2]. In 1980s, Japanese scholar Niihara [3] reported that mechanical properties of ceramics could be improved after addition of nano-powders [4–7]. From then on, nano-TiN powder was partially added into Ti(C,N)-based cermets to improve the toughness. Nowadays, TiN has been used as the main hard phase of Ti(C,N)-based cermets.

However, nano-TiN powder has two major drawbacks due to the large specific areas. Firstly, nano-TiN powders tend to aggregate spontaneously due to the large van der Waals attractive forces between the particles [8]. Inhomogeneous dispersion of the nano-TiN powders, such as flocculation and agglomeration, is detrimental to the properties of Ti(C,N)-based cermets [9]. Therefore, nano-TiN powder should be dispersed before added into the Ti(C,N)-based cermets matrix. Except for the well dispersion of the nano-TiN powder, there is another factor of great importance, i.e. the oxidation of nano-powder. Since nano-TiN powder has large specific areas, oxygen tends to be adsorbed on the surface. Furthermore, the wettability between the ceramic grains and liquid metal decreases due to the residual oxygen content on the surface of nano-powder. Therefore, large pores tend to form, and the densification course during the sintering process of nano-TiN doped Ti(C,N)-based cermets is inhibited [5].

At present, the deteriorating effect of oxygen contamination on the nano-TiN powder is well known. Many literatures reported that the oxygen content of micro-scaled powder can be successfully decreased by heating in vacuum [10,11]. However, little attention was paid on the microchemical and microstructural changes of nano-powder after vacuum heat treatment. Therefore, in this paper, nano-TiN powders were heat treated in vacuum to decrease the adsorbed oxygen. An emphasis was paid on the effect of vacuum heat treatment on the surface oxygen content, lattice parameter and morphology of the nano-TiN powder. The paper was a continuation and extension of our recent paper on nano-TiN powder [12].

2. Experimental procedures

Commercial available nano-TiN powder (Hefei Kaier Nanotechonlogy Development Co., Ltd., China) was used in the study. The nano-powder had an average particle size of 20 nm by TEM, a BET (Brunauer–Emmett–Teller) specific surface area of 80 m^2/g and oxygen content of 6.64 wt%.

* Corresponding author. Tel.: +86 13688313720; fax: +86 28 85196764.
E-mail address: submission001@hotmail.com (Z. Guo).

0925-8388/$ – see front matter © 2010 Elsevier B.V. All rights reserved.
doi:10.1016/j.jallcom.2010.07.045

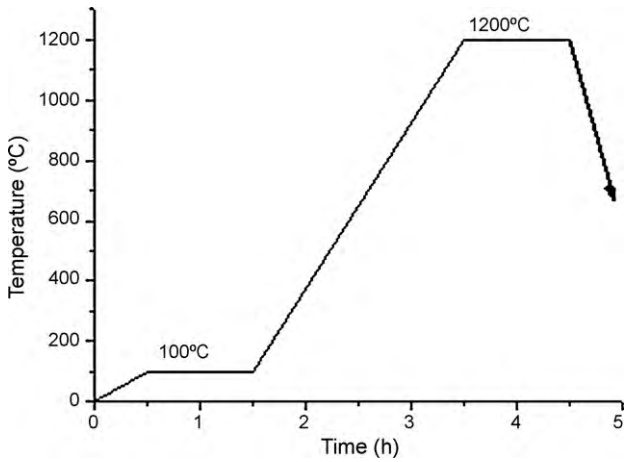

Fig. 1. Schematic of the vacuum heat treatment process.

The as-received nano-TiN powder was put into a graphite crucible, and then the crucible was put into a vacuum furnace of pilot scale. After achieving a vacuum degree of 0.5 Pa, the temperature was firstly increased from room temperature to 100 °C and held for 1 h to remove the possibly adsorbed H_2O molecules. Then the temperature was increased to 1200 °C and held for 1 h with a vacuum degree of 0.1 Pa, anticipating to decrease the oxide content of the nano-TiN powder at this stage. Fig. 1 shows the schematic of the vacuum heat treatment process.

The particle size distribution of the powders was measured by laser particle size analyzer (Malvern Mastersizer 2000, UK). Oxygen content of the nano-TiN powder was analyzed using oxygen–nitrogen instrument (Japan, HORIBA Company). Philips X'Pert Pro X-ray diffraction instrument (XRD, Holland) was used for phase analysis with Cu Kα Radiation. JEM-100CX Transmission Electron Microscope (TEM, JEOL, Japan) was used to observe the morphology. The surface composition of the nano-TiN powder was determined by X-ray photoelectron spectroscopy (XPS, XSAM800, Kratos Ltd., UK.) using MgKα (1253.6 eV) radiation. Survey spectra were collected in the energy range of 0–1000 eV at 1 eV/step, followed by a high-resolution scan at 0.1 eV/step. The spectra of the Ti_{2p}, N_{1s}, and O_{1s} peaks were calibrated according to the C_{1s} core level of as-received TiN at the energy of 284.8 eV. In this paper, atomic sensitivity factors of Ti_{2p}, O_{1s}, and N_{1s} were 1.20, 0.66 and 0.42, respectively. It should be noted that both the as-received and as-treated nano-TiN powder were characterized by the above techniques.

3. Results and discussion

3.1. Surface chemical composition

XPS was employed to investigate the surface chemical composition of the nano-TiN powder before and after vacuum treatment. Fig. 2 shows the high-resolution XPS spectra of as-received and as-treated nano-TiN powder. The deconvolution of the high-resolution spectra was performed with the Gaussian function. As for the N_{1s} spectrum shown in Fig. 2(a), the only peak at about 397 eV could be attributed to titanium nitride [13]. In the O_{1s} spectrum shown in Fig. 2(b), the peak at about 530 eV was assigned to titanium dioxide [13] and the peak at about 532 eV was assigned to oxygen [14]. There were four peaks in the Ti_{2p} core level spectrum shown in Fig. 2(c). The observed binding energy value of $Ti_{2p2/3}$ (at around 458 eV) and $Ti_{2p1/2}$ (at around 464 eV) agreed with the reported

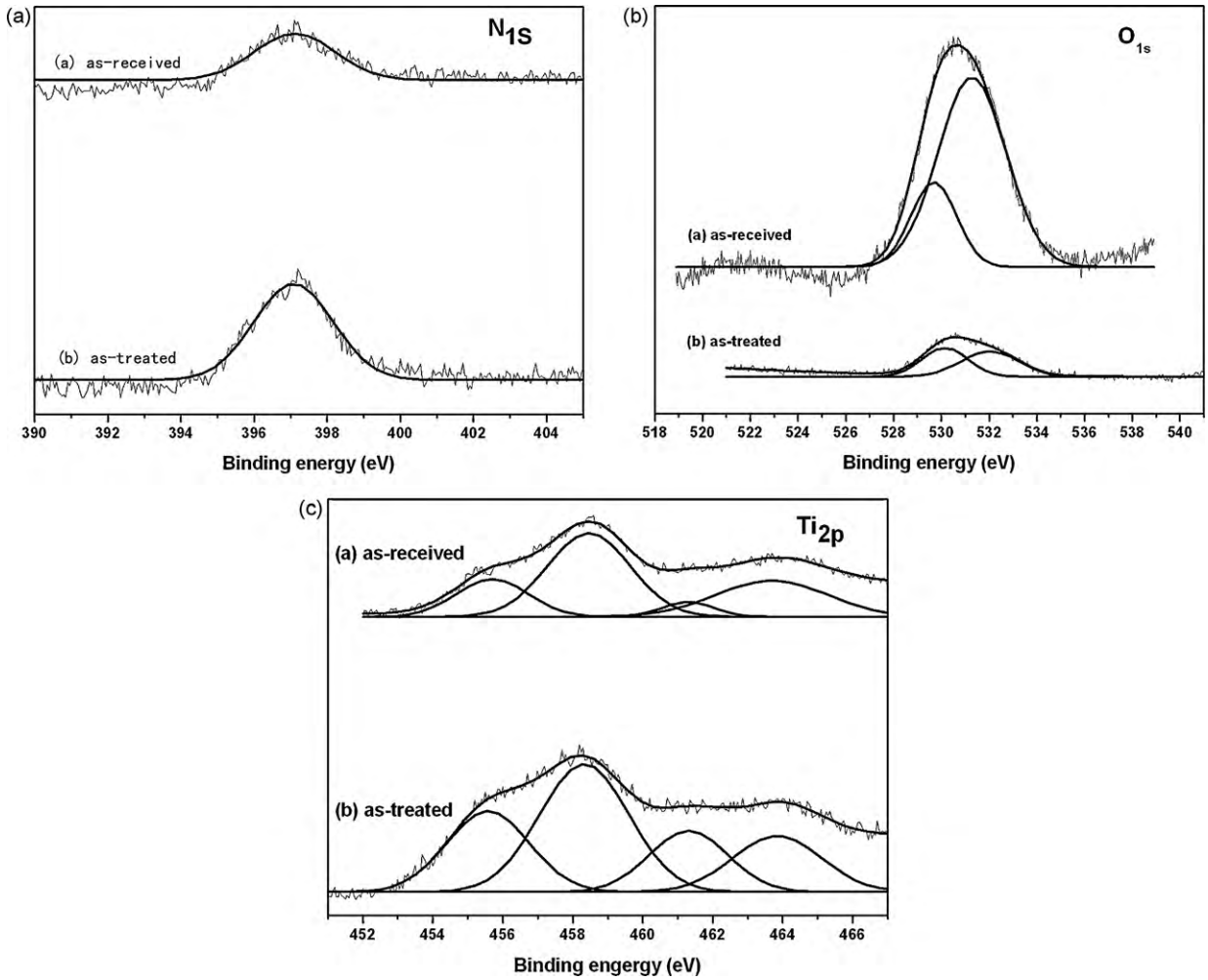

Fig. 2. High-resolution XPS spectra of as-received and as-treated nano-TiN powder. (a) N_{1s}, (b) O_{1s}, and (c) Ti_{2p}.

Table 1
Areas of all the peaks in the XPS spectrum of the as-received and as-treated nano-TiN powder.

Peaks	As-received powder		As-treated powder	
	Binding energy (eV)	Area (a.u.)	Binding energy (eV)	Area (a.u.)
$Ti_{2p2/3\,(TiN)}$	455.7	422	455.6	1037.2
$Ti_{2p2/3(TiO_2)}$	458.5	1077.9	458.3	1775.9
$Ti_{2p2/3\,(TiN)}$	461.3	118.8	461.3	748.4
$Ti_{2p1/2(TiO_2)}$	463.7	627.5	463.8	770.8
$O_{1s(TiO_2)}$	529.7	645.8	530.2	222.9
$O_{1s(O_2)}$	531.3	2167.1	532.0	245.3
N_{1s}	397.1	316.1	397.1	639.3

data for amorphous TiO_2 [15]. The binding energy value of $Ti_{2p2/3}$ (at around 455 eV) and $Ti_{2p1/2}$ (at around 461 eV) agreed with the reported data for TiN [15]. Substoichiometric oxide, as oxynitride TiO_xN_y reported by literature [16] did not appear in the nano-TiN of the paper. It could be concluded that the Ti_{2p}, O_{1s} and N_{1s} core levels indicated the presence of TiO_2, O_2 and TiN compositions on the surface of the as-received and as-treated nano-TiN powders.

However, the atom concentration ratios changed after vacuum heat treatment. The atom concentration ratio of O/Ti and N/Ti can be determined from the integrated peak areas of O_{1s}, N_{1s} and Ti_{2p} spectra listed in Table 1. It could be simply calculated that the atom concentration ratio of N/Ti remained at about 0.14, indicating that there was no decomposition of TiN during vacuum heat treatment. However, the atom concentration ratio of O/Ti was largely decreased from 1.25 to 0.11 after the vacuum heat treatment. Calculated from Table 1, the atom concentration ratio of $O_{1s}(O_2)/O_{1s}(TiO_2)$ decreased from 3.36 to 1.1. Furthermore, mixed valence titanium oxides, which can be written as $TinO_2n-1$ ($n \geq 2$), cannot be seen from Fig. 2. It can be deduced that the carbothermic reduction reaction of TiO_2 did not occur in the experiment, which occurs in the presence of carbon, especially carbon black, over a temperature range of 1700–2100 °C [17–18]. Therefore, it can be concluded that the phenomenon of oxygen content decrease can be largely attributed to the decrease of adsorbed oxygen other than combined oxygen.

The O and N content of the as-received and as-treated TiN powder were further tested by HORIBA oxygen–nitrogen instrument and the result was listed in Table 2. It can be seen that the N content was almost unchanged at about 22 wt% and the oxygen content decreased from 6.64 wt% to 1.18 wt%. The chemical analysis results proved the above analysis on the atom concentration ratio of O/Ti and N/Ti.

Table 2
Oxygen can nitrogen content of as-received and as-treated nano-TiN powder.

Powder		Oxygen (wt%)	Nitrogen (wt%)
As-received	Average value	6.64	22.3
	Standard deviation	0.03	0.03
As-treated	Average value	1.18	22.4
	Standard deviation	0.02	0.04

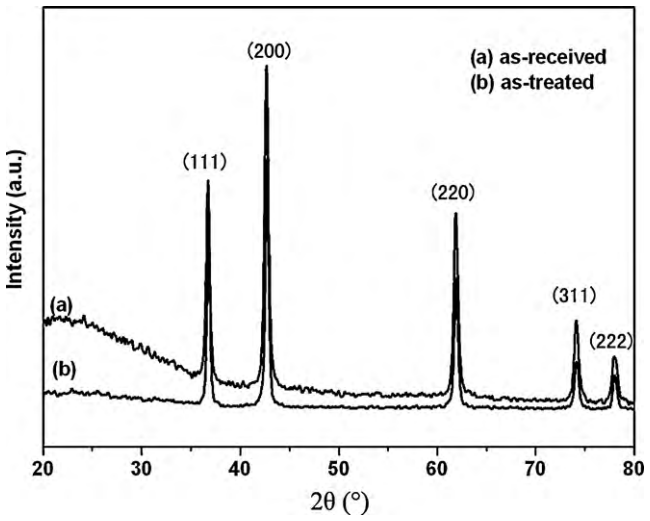

Fig. 3. XRD pattern of the as-received and as-treated nano-TiN powder.

3.2. XRD analysis

Fig. 3 shows the XRD patterns of nano-TiN powder before and after vacuum heat treatment process. It was clear that both the XRD pattern of as-received and as-treated nano-TiN powder exhibited five prominent peaks at various scattering angles, which could be assigned to the (1 1 1), (2 0 0), (2 2 0), (3 1 1) and (2 2 2) crystal planes ($a = b = c = 4.242$, JCPDS Card 38-1420), respectively. No obvious peaks for other impurities such as TiO_2 and TiO could be seen due to their low content. Apparently, the nano-TiN powder maintained the face-centered cubic structure (space group *Fm*-3*m*) without any distinct phase changes, indicating that the nano-TiN raw powder was stable during the vacuum heat treatment.

Fig. 4 shows the magnified view of the (1 1 1), (2 0 0), (2 2 0), (3 1 1) and (2 2 2) peaks of as-received and as-treated nano-TiN powder. It could be seen that all the peaks exhibited slight shift to higher angles after vacuum heat treatment, indicating the contraction of lattice. Furthermore, it could be seen that the patterns were less broad, indicating increase of crystallite size.

Table 3
The diffraction data and the calculated crystallite size and lattice parameter.

Powder	2θ (°)	d (Å)	(h k l)	FWHM (°)	Crystallite size (nm)	Lattice parameter (Å)
As-received	36.675	2.4484	1 1 1	0.408	21.2	4.2407
	42.669	2.1173	2 0 0	0.435	20.1	4.2345
	61.842	1.499	2 2 0	0.443	21.4	4.2398
	74.08	1.2787	3 1 1	0.527	19.2	4.2411
	77.948	1.2247	2 2 2	0.596	17.4	4.2424
		Average			19.86	4.2397
As-treated	36.808	2.4398	1 1 1	0.363	240	4.2259
	42.72	2.1148	2 0 0	0.355	250	4.2297
	61.892	1.4979	2 2 0	0.396	242	4.2368
	74.188	1.2771	3 1 1	0.485	210	4.2358
	78.058	1.2232	2 2 2	0.475	220	4.2373
		Average			23.24	4.2331

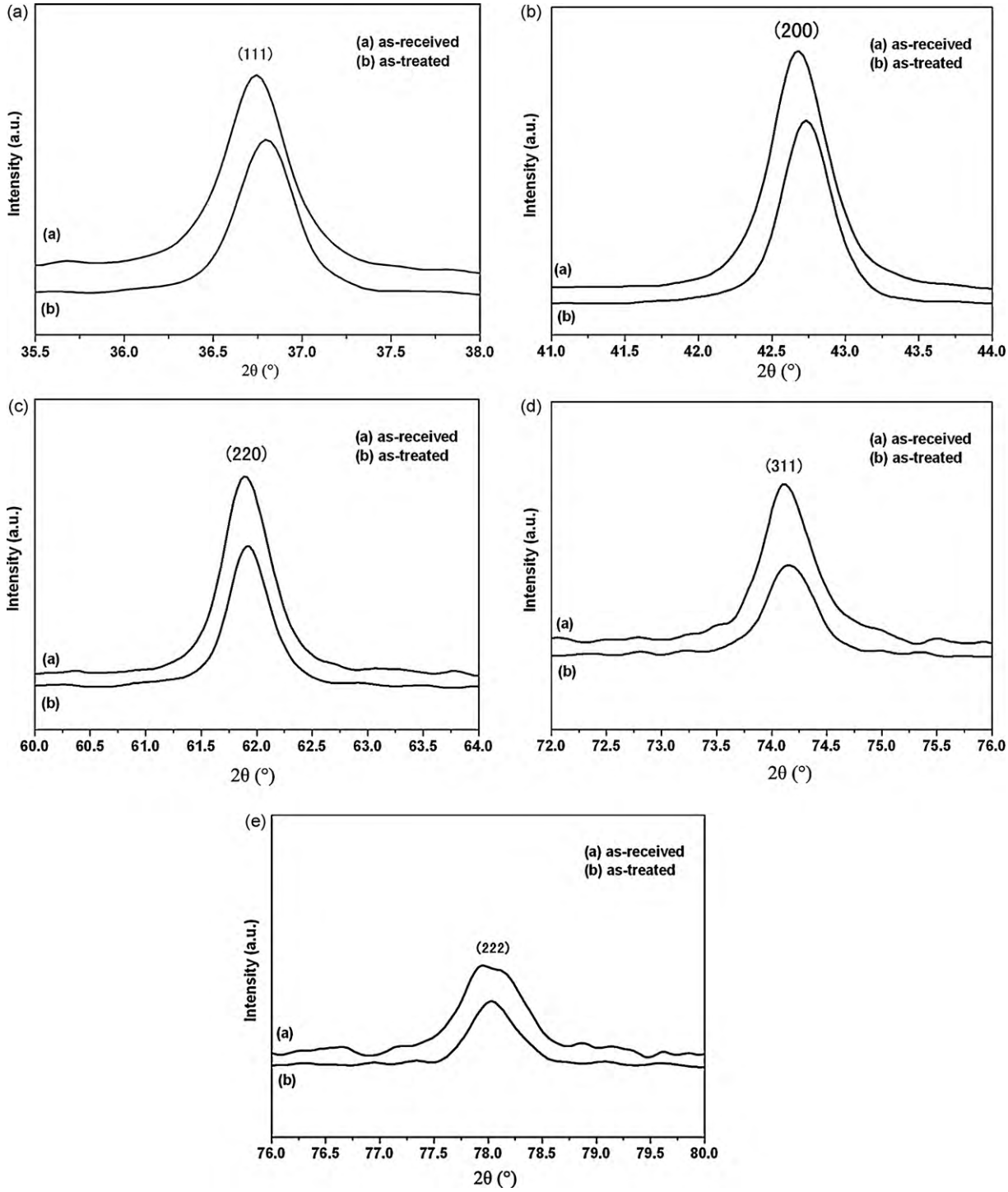

Fig. 4. Magnified view of the (1 1 1), (2 0 0), (2 2 0), (3 1 1) and (2 2 2) peaks of as-received and as-treated nano-TiN powder. (a) (1 1 1), (b) (2 0 0), (c) (2 2 0), (d) (3 1 1), and (e) (2 2 2).

Table 3 shows the diffraction data. According to the Bragg law for the cubic system [19] shown in formula (1), the precise lattice parameter of as-received and as-treated nano-TiN powder could be calculated from the diffraction data.

$$d = \frac{a}{\sqrt{h^2 + k^2 + l^2}} \quad (1)$$

where d is the lattice spacing, a is the lattice parameter, h, k, l are the Miller index of the crystal plane.

It could be seen from Table 3 that the average lattice parameter deceased from 4.2397 Å to 4.2331 Å, which may be due to the decrease of lattice defects during heat treatment.

Since the powder was heat treated in vacuum, taking no account of lattice strain broadening, the diffraction data could be analyzed based on the Scherrer formula [20], which is related to crystallite size:

$$D = \frac{K\lambda}{B \cos\theta} \quad (2)$$

Table 4
Volume ratio of as-received and as-treated TiN nano-powder in different particle size range.

Particle size range (μm)	0.02–0.2	0.2–0.4	0.4–0.6	0.6–0.8	0.8–1.0	>1.0
As-received (vol%)	25.45	61.48	13.06	0.01	0	0
As-treated (vol%)	32.9	18.37	1.98	0	0.34	46.41

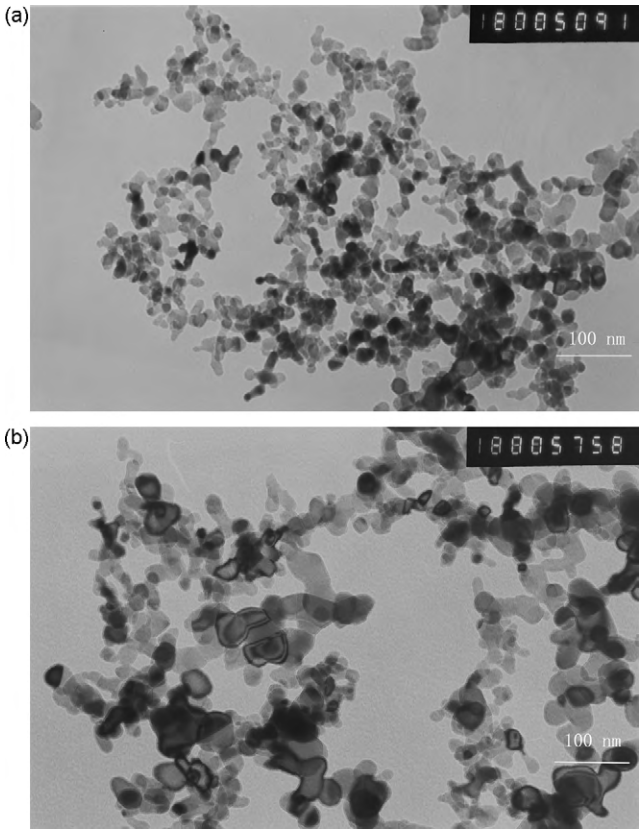

Fig. 5. TEM images of the as-received and as-treated nano-TiN powder. (a) As-received and (b) as-treated.

where D is grain size (nm); K is the Scherrer parameter (i.e. 0.89), λ is the X-ray wavelength (1.5406 Å), B is the full width at half maximum (FWHM) (rad), and θ is the Bragg angle.

It could be seen from Table 3 that the average crystallite size increased from 19.86 nm to 23.24 nm, which may be ascribed to the grain growth during heat treatment.

3.3. Morphology

Fig. 5 shows the TEM images of the as-received and as-treated nano-TiN powder. The as-received nano-TiN particles exhibited an elliptical shape with an average diameter of 20 nm. Irregularly shaped powder agglomerates with a diameter of 100 nm could be seen in Fig. 5(a). As shown in Fig. 5(b), the as-treated nano-TiN particles showed spherical shape with the average diameter increased to 40 nm. It could be concluded that the nano-TiN particles grew obviously at the high temperature. Agglomeration of the nano-particles appeared to be more serious, and the diameters of these agglomerates were estimated to reach several hundreds of nanometers. The TEM images verified the XRD analysis on the grain growth. Table 4 shows the particle size distribution of as-received and as-treated nano-TiN powder. It could be seen that the as-received nano-TiN powder had a narrow size distribution, but the as-treated powder had a wider size distribution and much more particles were in the range of above 1 μm. The TEM image and particle size analysis indicated the sintering behavior of nano-TiN powder during the vacuum heat treatment process.

4. Conclusions

In the paper, the nano-TiN powder was heat treated in vacuum at 1200 °C for 1 h to decrease the oxygen content of the nano-powder. The oxygen content, the crystalline size and the morphology were characterized before and after the process. The oxygen content of the nano-TiN powder could be largely decreased from 6.64 wt% to 1.18 wt% by the vacuum heat treatment. However, the average particle size increased from 20 nm to 40 nm from TEM, and there was a slight decrease of lattice parameter from 4.2397 Å to 4.2331 Å by XRD.

Acknowledgements

The study is financially supported by National Natural Science Foundation of China (No. 50874076) and the Ministry of Science and Technology of China (No. 2009GJF00030). The authors are grateful to Chengdu Mingwu Technology Corp., Ltd. of China for supply of materials. Thanks are also extended to Analytical & Testing Center of Sichuan University for the testing of the samples.

References

[1] S. Kang, Powder Metall. 40 (1997) 139–142.
[2] H. Pastor, Mater. Sci. Eng. A 105/106 (1988) 401–409.
[3] K. Niihara, Powder Metall. 44 (1997) 887–896.
[4] X.B. Zhang, N. Liu, Int. J. Refract. Met. H 26 (2008) 575–582.
[5] Y. Zheng, W.H. Xiong, W.J. Liu, W. Lei, Q. Yuan, Ceram. Int. 31 (2005) 165–170.
[6] N. Liu, Y.D. Xu, H. Li, G.H. Li, L.D. Zhang, J. Eur. Ceram. Soc. 22 (2002) 2409–2414.
[7] N. Liu, Y.D. Xu, H. Li, Z.H. Li, Y. Zhao, G.H. Li, et al., Mater. Sci. Technol. 18 (2002) 586–590.
[8] B.J. Briscoe, A.U. Khan, P.F. Luckham, J. Eur. Ceram. Soc. 18 (1998) 2141–2147.
[9] C.J. Shih, B.H. Lung, M.H. Hon, Mater. Chem. Phys. 60 (1999) 150–157.
[10] Y. Zhao, C.L. Wang, K.N. Yang, Powder Metall. Technol. 21 (2003) 145–150.
[11] M.S. Wang, X.Y. Song, S.X. Zhao, J. Funct. Mater. 38 (2007) 1519–1522.
[12] Z.G. Guo, J. Xiong, Mei Yang, S.J. Xiong, J.Z. Chen, Y.M. Wu., et al., J. Alloys Compd. 493 (2010) 362–367.
[13] N.C. Saha, H.G. Tompkins, J. Appl. Phys. 72 (1992) 3072–3079.
[14] M.Z. Atashbar, H.T. Sun, B. Gong, W. Wlodarski, R. Lamb, Thin Solid Films 326 (1998) 238–244.
[15] F.H. Lu, H.Y. Chen, Thin Solid Films 355–356 (1999) 374–379.
[16] J.X. Zhang, L.P. Duan, D.L. Jiang, Q.L. Lin, M. Iwasa, J. Colloid Interface Sci. 286 (2005) 209–215.
[17] N. Setoudeh, A. Saidi, N.J. Welham, J. Alloys Compd. 390 (2005) 138–143.
[18] N. Setoudeh, A. Saidi, N.J. Welham, J. Alloys Compd. 419 (2006) 247–250.
[19] Y.X. Li, J.D. Hu, H.Y. Wang, Z.X. Guo, A.N. Chumakov, Mater. Sci. Eng. A 458 (2007) 235–239.
[20] A.M. Hindeleh, D.J. Johnson, Polymer 21 (1980) 929–935.